Development of a Novel Backup Fault Protection Algorithm for Low-Voltage DC Microgrids based on Local Measurements and Chi-square Statistics

Duong Minh Bui
Department of Electrical and Computer Engineering, Faculty of Engineering, Vietnamese-German University (VGU), Binh Duong, Vietnam
duong.bm@vgu.edu.vn

Phuc Duy Le
Faculty of Electrical Engineering Technology, Industrial University of Ho Chi Minh City, Ho Chi Minh City, Vietnam
phucld91@gmail.com (corresponding author)

Hieu Minh Nguyen
Department of Electrical and Computer Engineering, Faculty of Engineering, Vietnamese-German University (VGU), Binh Duong, Vietnam
hieu.nm@vgu.edu.vn

Received: 6 February 2024 | Revised: 13 May 2024 | Accepted: 15 May 2024

 DOI: https://doi.org/10.48084/etasr.7022

ABSTRACT

A direct-current microgrid (MG) can be susceptible to extremely high fault currents contributed by the output filter capacitors of power converters and can also face protection challenges because of the non-zero crossing of fault currents. In a Low-Voltage Direct Current (LVDC) MG, low-fault-tolerance converters such as boost converters and bidirectional converters mostly require a fast and adaptable fault protection scheme that can detect and clear quickly faults irrespective of a wide range of fault impedances in the system. Several current- and voltage-derivative-based protection methods with communication support have been developed to primarily protect DC MGs due to their high sensitivity and selectivity. Over-current and under-voltage-based protection schemes are mostly suggested as backup protections for the DC MGs. To accurately detect and rapidly clear the faults even in the case of communication failure from the primary protection, this paper proposes a novel backup fault protection scheme with high selectivity, adaptability, and scalability for islanded LVDC MGs based on local measurements along with Chi-square-distribution-based statistics. Specifically, this developed backup protection not only applies a cumulative summation methodology for the locally measured signals to extract derivative and integral characteristics of the current and voltage, but also uses the Chi-square-distribution-based statistics to consistently calculate tripping thresholds for the effective detection of different fault events in the LVDC MG, regardless of variable fault resistances and the communication-link damage. As a result, the proposed backup protection is capable of accurately detecting various DC faults to secondarily protect the source and load branches of the system within the expected time frame of a few milliseconds and has been validated through multiple staged fault tests from an off-grid and ungrounded 1kW and 48V_{DC} MG testbed.

Keywords-chi-square; current derivative; current integral; fault protection; local measurement; voltage derivative

I. INTRODUCTION

Advanced technologies of Renewable Energy Sources (RESs) have allowed the wide development of Low-Voltage Direct Durrent (LVDC) microgrids (MGs). An LVDC MG can operate in a grid-connected mode in which it can share its load and generation with a main grid, or in an islanded mode in which the MG can sustain itself [1]. To harness RESs, different

types of power converters are used depending on the type of RES. These power converters can be susceptible to pole-to-pole (P2P) or pole-to-ground (P2G) faults in the DC MG due to their low fault-tolerance characteristic and extremely high fault currents from DC-link or filter capacitors in the system. Furthermore, fault impedances in the LVDC MG can vary greatly, reducing the accuracy and adaptability of several protection schemes based on the magnitudes of fault current and voltage [2-5]. Therefore, it is imperative to develop a fast and adaptable fault protection scheme to quickly remove the fault regardless of low or high fault impedances in the LVDC microgrid.

Several protection algorithms for LVDC MGs have been developed, which are categorized into unit and non-unit protection methods with high requirements of selectivity, adaptability, sensitivity, reliability, and speed [6]. In general, non-unit protection methods are based on the pre-determined tripping threshold violation and have no division of protected zones in the DC MG [7, 8]. However, these protection schemes may be ineffective in cases of relatively high fault resistance and have low selectivity due to difficulties in locating the faults in the MG [9]. Therefore, Over-Current (OC) and Under-Voltage (UV)-based protection schemes are mostly suggested as backup protections for the MG. On the other hand, unit protection methods are used to improve the sensitivity and adaptability of the DC MG protection, which will divide a DC-microgrid configuration into multiple protection zones/lines [10]. The data exchange between the protected zones is supported by a communication network. In [11-13], various DC faults can be detected timely using the high rate of change in current/voltage and are correctly located by comparison of the slopes of current/voltage between adjacent protective devices in the system under the communication support. Other unit protection schemes can be differential-current-based methods [14, 15], event-based methods [11, 16], blocking-based methods [17], and protection methods based on S-transform, positive, negative, and zero sequences of current and voltage waveforms to respond to all dynamic topologies of the MG [18, 19]. In [11, 16], event-based protection methods are suggested to reduce the communication bandwidth requirements. Specifically, a protective relay can classify the local and remote faults under different events in the MG and then communicate with other relays for protection coordination. Only the event-based decisions need to be transmitted among the corresponding relays to reduce the communication data rate and time delay. In [8], a communication-based directional OC and differential protection scheme is proposed for the DC MG with multiple DG units.

To reduce the dependence of communication links on the DC-MG protection, as mentioned in [20-22], only the current response from the one side of the trunk line is measured to protect it in the DC-MG configuration. A central protective relay is used to perform the protection of pre-defined line segments in the system or OC and current-directional/differential-comparison-based protection schemes with communication links are incorporated for protecting the generator and the load units in the DC MG, respectively. However, fault detection based on the directional OC characteristic requires additional hardware circuitry for protection coordination and faster communication time. In [23], a fault detection method based on the difference in the Teager energy in current waves is proposed to protect lines in the DC MG. In [24], the directional OC protection method with K-means clustering is studied to define setting groups of the OC relays in the MG and use the IEC61850 communication protocol. In [25, 26], differential-current-derivative-based fault detection and location methods utilizing machine learning algorithms are proposed for the LVDC MG, however, training data collection corresponding to several random fault events, such as different fault impedances, fault locations, network topologies, penetration of distributed generators, volatile nature of renewable energy sources, and MG operating modes, may be difficult to be practically performed in real-time.

For the protection of the DC-link or common DC-bus of the DC MG, a fault detection and isolation scheme using over-/under-voltage protection functions has been commonly applied in the system [27]. In [28], a rapid DC-fault detection method is proposed by analyzing the similarity between the sampled abnormal current and the steady-state current through an improved Pearson correlation coefficient. However, this method may not be effectively applied to high-impedance faults. In [29, 30], the transient-monitoring-function or resistance-estimation-based fault detection methods are developed for DC MGs in order to decrease the required bandwidth of the communication channels and eliminate the synchronization error. However, they may not be effectively applied to close-in faults or low fault-tolerance power converters in the MG. In [21, 31-34], local-measurement-based protection methods are developed for the islanded DC MG by using OC relays, analyzing the fault response time and estimating the resistance from the relay position to the faulted point. However, the determination of tripping/pick-up current thresholds will be the protection challenge if this study is only based on empirical factors. Therefore, it may be necessary to use statistical methods to effectively determine the tripping thresholds of the OC/UV protection of the DC MG. In [35], an adaptive statistical fano-factor-tool-based scheme was developed to detect and classify various DC faults with enhanced noise-tolerance capability through the collection of the current data at the line ends. However, this fault detection scheme is only validated by simulation results. There are other DC-MG protection methods, such as the fuse-based short-circuit protection strategy for converter-controlled LVDC MGs [36], the oscillation-frequency-based fault identification scheme under di/dt conditions [37], and the fault detection method based on real and imaginary fast-Fourier-transform powers [38]. However, they could not be effective in high-impedance fault detection or accurate classification between various faults and other abnormal conditions of the DC MG operation.

In summary, unit protection methods, e.g. current/voltage derivative-based protection methods with communication support, are commonly proposed to protect the DC MG due to their high reliability and selectivity, requiring the synchronization of measurement devices due to the fast change of current and voltage. In the case of communication failure, backup protection schemes must be activated to protect the

source and the load branches in the DC MG. However, in order to ensure high selectivity and adaptability of backup protection, this paper proposes a novel backup protection scheme based on local measurements and Chi-square statistics for LVDC MG to timely detect and clear the DC faults irrespective of variable fault resistances and damage of the communication system. Specifically, this developed backup protection utilizes locally measured signals to extract derivative and integral characteristics of current and voltage and set up Chi-square-based tripping thresholds for identifying different fault events in the LVDC MG. In general, the main contributions of this paper are:

- The development of a novel backup fault protection for small-scaled LVDC MGs based on local measurements of the current and voltage at the source and load branches without communication support.
- The use of Chi-square-distribution-based thresholds to detect the abnormal operation of the LVDC MG with high selectivity.
- The use of the Cumulative Summation (CS) algorithm to analyze the sampling data of fault current and voltage and determine the adaptable fault-tripping thresholds for the protection with high adaptability and scalability. Typically, the CS algorithm calculates the integration of difference between the actual measured/sampled value and its mean value with respect to a definite time duration to reduce the noise from non-fault transient operations in the DC system. Therefore, the CS algorithm has enhanced noise-tolerance capability and can adapt to both close-in or far-away faults from the source in the converter-controlled DC MGs.
- Quick detection and localization of severe short-circuit faults within a few milliseconds.
- Less sensitivity to spurious spikes of the measured system.

The proposed protection method is capable of accurately detecting the DC faults to protect source and load branches within the expected time frame and has been validated through multiple staged fault tests, e.g. fault tests with different fault impedances, fault tests at various faulted locations, network topologies with penetration of photovoltaic (PV) energy sources, and MG islanded operating modes, from a real-time ungrounded 1 kW and 48 V_{DC} MG testbed.

II. TRANSIENT BEHAVIORS OF AN LVDC MG FROM DIFFERENT DC FAULT TYPES

A. Different Fault Types and Locations in an LVDC MG

Figure 1 shows an ungrounded LVDC MG with a PV-energy-source branch, a Battery-Energy-Storage-System (BESS) branch, and a DC-load branch. With small-sized LVDC MGs, a direct grounding system is not usually used in such a way that the DC MG can get the effective cost and properly separate from the grounding system of the utility grid. The different faulted locations in the studied LVDC MG are: the DC common bus (F1), the terminal of battery packs (F2), and the DC-load side (F3). P_1, P_2, P_3, P_4, and P_5 are protective devices utilized in the MG. P2P or P2G faults can occur at these locations, however, the P2P faults are more serious than the P2G faults because the mentioned LVDC MG configuration is ungrounded. Thus, if a P2G fault randomly occurs at the positions F1, F2, or F3 in the ungrounded DC MG as seen in Figure 1, the P2G fault current is mostly considered as the leakage current, which may insignificantly affect the continuous operation of the MG. In general, it is possible to detect P2G faults, e.g. positive (+)-pole or negative (-)-pole to the ground, based on over-voltage characteristics or the rate of change of voltage at the negative or positive line of the DC MG, respectively.

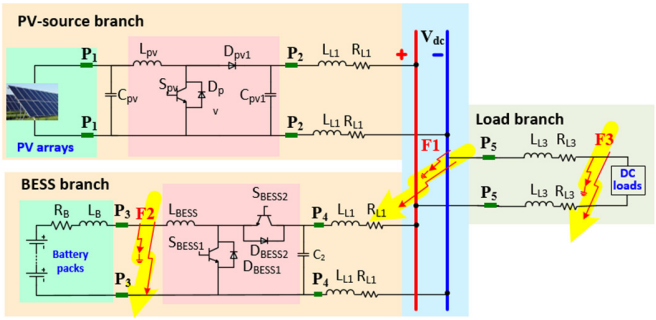

Fig. 1. An ungrounded and islanded LVDC MG with a PV-source branch, a BESS branch, and a DC-load branch.

B. Derivative and Integral Characteristics of Fault Current at the Most Serious Location – a DC Common Bus (F1)

When a short-circuit occurs at the DC common bus (F1), as noticed in Figure 2, regardless of the converter type (DC-DC boost converters or bidirectional DC-DC converters), the fault current $i_{L,s}(s)$ contributed by the output filter capacitors at the fault inception time t_0 can be expressed in the frequency domain [39]:

$$i_{L,s}(s) = \frac{v_{C,s}(0)/L_{eq} + i_{L,s}(0)s}{s^2 + \frac{R_{eq}}{L_{eq}}s + \frac{1}{L_{eq}C_{eq}}} \quad (1)$$

$$R_{eq} = 2R_{L1} + R_f;\ L_{eq} = 2L_{L1} \quad (2)$$

where the subscript s represents the PV source branch and $BESS$ represents the BESS branch in the studied MG, $v_{C,s}(0)$ and $i_{L,s}(0)$ are the initial values of the output capacitor voltage and the line current, respectively, at the inception time t_0, R_{eq} and L_{eq} are the equivalent series resistance and inductance respectively from the output capacitor to the faulted position (F1) as seen in Figure 2, R_f is the fault resistance in the MG system, and C_{eq} is the equivalent capacitance at the power converter's output.

The line current $i_{L,s}(t)$ in the time domain is expressed as in (3), where p_1 and p_2 are the poles of (1). It can be noted that the transient response of the line current significantly depends on the fault impedance and the distance from the power converter output to the faulted position in the system. The real/complex values of p_1 and p_2 depend on the comparison between ω_0^2 and α^2, as mentioned in (5). If ω_0^2 is less than, greater than, or equal to α^2, then the fault current

characteristic will be under-damped, over-damped, or critically damped, respectively. In addition, by differentiating the line fault current from (3) with respect to time, the rate of current change is expressed as in (6).

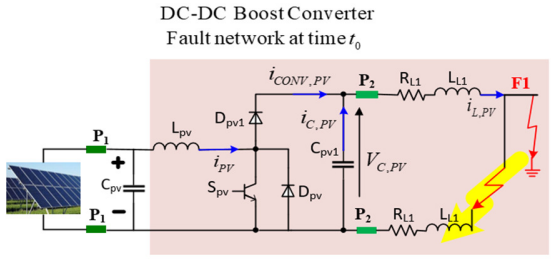

(a) Fault network of the boost converter at the inception time t_0.

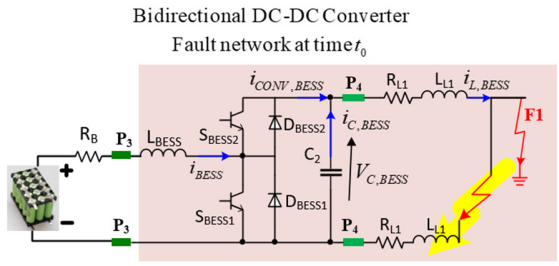

(b) Fault network of the bidirectional converter at the time t_0.

Fig. 2. Equivalent circuit of the converters in the DC MG under the short-circuit fault at F1.

$$i_{L,s}(t)=\frac{v_{C,s}(0)}{L_{eq}(p_2-p_1)}\left[e^{-p_1t}-e^{-p_2t}\right]+\frac{i_{L,s}(0)}{p_2-p_1}\left[-p_1e^{-p_1t}+p_2e^{-p_2t}\right] \quad (3)$$

$$p_1,p_2=\frac{R_{eq}}{2L_{eq}}\pm\sqrt{\left(\frac{R_{eq}}{2L_{eq}}\right)^2-\frac{1}{L_{eq}C_{eq}}} \quad (4)$$

$$p_1,p_2=\alpha\pm\sqrt{\alpha^2-\omega_0^2}$$
$$\alpha=\frac{R_{eq}}{2L_{eq}} \quad (5)$$
$$\omega_0=\sqrt{\frac{1}{L_{eq}C_{eq}}}$$

$$\frac{di_{L,s}(t)}{dt}=\frac{v_{C,s}(0)}{L_{eq}(p_2-p_1)}\left[-p_1e^{-p_1t}+p_2e^{-p_2t}\right]+\frac{i_{L,s}(0)}{p_2-p_1}\left[p_1^2e^{-p_1t}-p_2^2e^{-p_2t}\right] \quad (6)$$

The rate of instant change in the current right after the fault inception time $t=0^+$ is expressed as:

$$\frac{di_{L,s}(0^+)}{dt}=\frac{v_{C,s}(0^-)-R_{eq}i_{L,s}(0^-)}{L_{eq}} \quad (7)$$

where $v_{C,s}(0^-)$ and $i_{L,s}(0^-)$ are the pre-fault voltage and line current, respectively, and $di_{L,s}(0^+)/dt$ is the current derivative determined instantaneously after the fault occurrence [40]. The parameter $di_{L,s}(0^+)/dt$ significantly decreases when the line loading $i_{L,s}(0^-)$ is high and the fault resistance is large. In addition, $di_{L,s}(0^+)/dt$ gets its minimum value when the fault distance is long.

By integrating the line fault current from (3) with respect to time t, an area A created by the fault current in a specific time duration can be expressed as:

$$A=\int_0^t i_{L,s}(t)dt=\frac{C_{eq}v_{C,s}(0)}{(p_2-p_1)}\left[-p_2e^{-p_1t}+p_1e^{-p_2t}+(p_2-p_1)\right]+\frac{i_{L,s}(0)}{p_2-p_1}\left[e^{-p_1t}-e^{-p_2t}\right] \quad (8)$$

Assuming that the short-circuit event happens at $t=0$, the integration of the current with $t: 0\rightarrow\infty$ is expressed as:

$$\int_0^\infty i_L(t)dt=C_{eq}v_{C,s}(0) \quad (9)$$

It can be noted that the current integral is not affected by the transient response of the short-circuit current, i.e. over-damping and under-damping conditions. Additionally, the current integral approaches $C_{eq}v_{C,s}(0)$ as $t\rightarrow\infty$. Moreover, in contrast to the current derivative, the current integral is also not affected by any fault parameter, i.e. fault resistance R_f, fault distance, and the initial line current $i_{L,s}(0)$. Generally, the current integral is only dependent on the initial voltage across the converter's output capacitor $v_{C,s}(0)$.

C. Derivative and Integral Characteristics of Fault Voltage at the DC Common Bus (F1)

Considering the voltage response of the converters' output capacitor in the DC MG over the faulted period, the fault voltage is proportional to the current integral.

- For underdamped conditions of the fault event:

$$v_{C,s}(t)=v_{C,s}(0)e^{-\alpha t}\left[\cos(\omega_d t)+\frac{\alpha}{\omega_d}\sin(\omega_d t)\right]+\frac{i_{L,s}(0)}{\omega_d C_{eq}}e^{-\alpha t}\sin(\omega_d t) \quad (10)$$

$$\omega_d=\sqrt{\omega_0^2-\alpha^2}=\sqrt{\frac{1}{L_{eq}C_{eq}}-\left(\frac{R_{eq}}{2L_{eq}}\right)^2} \quad (11)$$

- For overdamped conditions of the fault event:

$$v_{C,s}(t)=\frac{v_{C,s}(0)\omega_0^2}{(p_2-p_1)}\left(-\frac{e^{-p_1t}}{p_1}+\frac{e^{-p_2t}}{p_2}\right)+\frac{i_{L,s}(0)}{C_{eq}(p_2-p_1)}\left(e^{-p_1t}-e^{-p_2t}\right) \quad (12)$$

By differentiating the fault voltage from (10) and (12) with respect to time, the rate of voltage change is expressed by:

- For underdamped conditions of the fault event:

$$\frac{dv_{C,s}}{dt}=\frac{v_{C,s}(0)\omega_0^2}{\omega_d}e^{-\alpha t}\sin(\omega_d t)+\frac{i_{L,s}(0)}{C_{eq}}e^{-\alpha t}\left[-\frac{\alpha}{\omega_d}\sin(\omega_d t)+\cos(\omega_d t)\right] \quad (13)$$

- For overdamped conditions of the fault event:

$$\frac{dv_{C,s}}{dt}=\frac{v_{C,s}(0)\omega_0^2}{(p_2-p_1)}\left(e^{-p_1t}-e^{-p_2t}\right)+\frac{i_{L,s}(0)}{C_{eq}(p_2-p_1)}\left(-p_1e^{-p_1t}+p_2e^{-p_2t}\right) \quad (14)$$

The rate of instant change in voltage right after the fault inception time $t=0^+$, $dv_{C,s}(0^+)/dt$, is relatively small at $i_{L,s}(0^-)/C_{eq}$ and will be very high after a certain fault duration irrespective of the over-damping and under-damping conditions. The rate of voltage change $dv_{C,s}/dt$ significantly depends on the square of the resonant radian frequency ω_0^2, with $\omega_0^2=1/(L_{eq}C_{eq})$, the fault distance from the converter up to the faulted location, the fault impedance, and the initial values of $v_{C,s}(0)$ and $i_{L,s}(0)$. In addition, the parameter $dv_{C,s}(0^+)/dt$ substantially increases when the pre-fault line loading $i_{L,s}(0^-)$ is high and the filter capacitance C_{eq} is small.

By integrating the fault voltage from (10) and (12) with respect to time, an area *B* created by the fault voltage in a specific time duration can be expressed as in (15) according to different damping conditions in the DC system.

$$B=\int_0^t v_{C,s}(t)dt=\frac{v_{C,s}(0)\omega_0^2}{(p_2-p_1)}\left(\frac{1}{p_1^2}e^{-p_1t}-\frac{1}{p_2^2}e^{-p_2t}+\frac{1}{p_2^2}-\frac{1}{p_1^2}\right)+\frac{i_{L,s}(0)}{C_{eq}(p_2-p_1)}\left(-\frac{1}{p_1}\left(e^{-p_1t}-1\right)+\frac{1}{p_2}\left(e^{-p_2t}-1\right)\right) \quad (15)$$

It can be seen that area *B* will be very high right after the first time intervals of the fault event and then it gradually decreases for the next time intervals. Assumed that the short-circuit event happens at the time $t=0$, so the integration of the voltage with $t: 0\rightarrow\infty$ is expressed as in (16).

$$B=\int_0^\infty v_{C,s}(t)dt=\frac{i_{L,s}(0)}{L_{eq}C_{eq}^2}-\frac{v_{C,s}(0)R_{eq}}{L_{eq}^2C_{eq}} \quad (16)$$

In other words, the voltage integral is significantly affected by the transient response of the short-circuit voltage, i.e. the over-damping and under-damping conditions. Moreover, the voltage integral with $t: 0\rightarrow\infty$ is also influenced by any fault parameters, i.e. fault resistance R_f, fault distance, filter capacitance, the initial current $i_{L,s}(0)$, and the initial voltage $v_{C,s}(0)$. Therefore, the use of only the voltage derivative could be more feasible and proper to identify the short-circuit cases in the DC system than the use of the voltage integral or the use of both the voltage derivative and integral.

D. Frequency Domain Analysis of the Integration of Short-Circuit Current and Voltage at the Faulted Location F1

It is necessary to clear the short-circuit events as soon as possible, so it is not appropriate to analyze the short-circuit current/voltage integral with the time $t: 0\rightarrow\infty$. In other words, the value of the current integral will be less than $C_{eq}v_{C,s}(0)$ and that of the voltage integral will also be different from the value of $\left(i_{L,s}(0)/L_{eq}C_{eq}^2\right)-\left(v_{C,s}(0)R_{eq}/L_{eq}^2C_{eq}\right)$. Hence, the current or voltage integral in a discrete form can be expressed as in (17):

$$\begin{cases}\int_0^t i_{L,s}(t)dt=\sum_{j=1}^{n}i_{L,s,j}\\ \int_0^t v_{C,s}(t)dt=\sum_{j=1}^{n}v_{C,s,j}\end{cases} \quad (17)$$

where $n\ (=f_st)$ is the number of samples according to the sampling frequency f_s and t is the sampling time interval. The difference between the actual measured/sampled value and its mean value can be integrated with respect to a definite time duration to reduce the noise from non-fault transient operations in the DC system:

$$\begin{cases}\int_0^t\left(i_{L,s}(t)-\mu_i\right)dt=A_i(t)\\ \int_0^t\left(v_{C,s}(t)-\mu_v\right)dt=B_v(t)\end{cases} \quad (18)$$

where μ_i and μ_v are the mean of the functions $i_{L,s}(t)$ and $v_{C,s}(t)$, respectively, during the time interval $(0,t]$. To analyze the fault current and voltage sampling data and determine the adaptable fault-tripping thresholds for DC MG protection, a CS algorithm is proposed in the discrete forms of (18) as analyzed above. The CS algorithm is developed to get the enhanced noise-tolerance capability of the protection system and be adaptable to both close-in or far-away faults from the source in the converter-controlled DC MGs.

E. P2P Fault Analysis at the Battery (F2) and Load (F3) Branches in the Typical DC Microgrid

When a P2P fault (or a short-circuit fault) occurs at the load branch (F3) in the LVDC MG as shown in Figure 1, the fault responses of the PV-source branch and the BESS branch are similar to their responses in the case of the faulted location F1.

However, it is necessary to consider further the line resistance and inductance, R_{L3} and L_{L3}, as observed in Figure 1, which will significantly impact the exponential damping coefficient and the natural and resonant frequencies on the transient behaviors of fault current and voltage in the DC electric circuit. In addition, when a P2P fault happens at the terminal of battery packs (F2) as indicated in Figure 1, the battery fault current, $i_{Bat}(t)$, is calculated by:

$$i_{Bat}(t) = \frac{v_{Bat}(0)}{R_B}\left(1 - e^{-t\left(\frac{R_B}{L_B}\right)}\right) \quad (19)$$

where R_B and L_B are the internal resistance and inductance of the battery source, respectively, and $v_{Bat}(0)$ is the battery's initial voltage just before the fault occurrence. Protection devices, P_3, working as fast-acting DC fuses are commonly used to protect the battery packs in the GM system.

F. P2G Fault Analysis at Locations F1, F2, and F3

A standalone and small-sized LVDC MG is mostly ungrounded, so if a pole-to-ground fault occurs at F1, F2, or F3 in the DC MG as depicted in Figure 1. The P2G fault current can only be considered the DC leakage current which may insignificantly affect the continuous operation of the MG. In general, it is possible to identify the negative/positive-P2G faults based on over-voltage characteristics or the rate of change of voltage at the positive or negative line of the DC MG. The voltage measurement/sampling at the positive and negative poles of the LVDC MG can be implemented by creating a middle point of two series-connected capacitors at the DC-common bus to get the common voltage; hence, the positive-pole voltage is the potential difference between the (+) pole and the middle point of the DC-link capacitors, while the negative-pole voltage is the potential difference between the (-) pole and this middle point in the MG.

III. THE PROPOSED SCHEME

A backup fault protection scheme based on local measurements and Chi-square statistics for islanded LVDC MGs is proposed in this study, with the following main characteristics:

- In order to improve the selectivity of the protection, Chi-square-distribution-based thresholds of current and voltage derivatives are calculated to detect abnormal operation cases of the MG.
- In order to enhance the adaptability and scalability of the protection, a CS algorithm is developed to analyze the local sampling data of fault current and voltage and then determine the adaptable fault-tripping thresholds for the DC MG protection.
- The backup protection scheme with less sensitivity to the noise of the local measuring system can accurately detect and quickly clear severe short-circuit faults within a few milliseconds to protect source and load branches in which failures of circuit breakers or primary protection functions occur.

A. Abnormal Operation Detection for the LVDC MG based on Current and Voltage Derivatives

As indicated in Figure 3, the Stage 1 of the proposed backup protection algorithm is to detect abnormal operations of the LVDC MG. The rates of change of current and voltage, di_i/dt and dv_i/dt, are measured and compared to their Chi-square statistical thresholds in order to identify any abnormal operation of the MG system. Specifically, if the rates of change of current or voltage, as expressed in (20), exceed their Chi-square statistical threshold as shown in (21) and (22), then the algorithm will consider this an abnormal operation case. In (20), the subscript i is the i^{th} sampling order of current and voltage signal, Δt is the sampling time interval of the signals, selected to 0.001 s. For the one-sided confidence interval of the current derivative or the voltage derivative, the Chi-square statistical thresholds of the current and the derivatives $\chi^2\{di/dt\}_{n-1,1-\alpha}$ and $\chi^2\{dv/dt\}_{n-1,1-\alpha}$ can be expressed as in (21) and (22), where n is the total number of samples used for the Chi-square distribution, selected to 100 samples and the subscript $(1-\alpha)$ is the confidence coefficient of the distribution, selected to 95%.

$$\frac{di_i}{dt} = \frac{i_i - i_{i-1}}{\Delta t} \;\&\; \frac{dv_i}{dt} = \frac{v_i - v_{i-1}}{\Delta t} \quad (20)$$

$$\chi^2\{di/dt\}_{n-1,1-\alpha} = \mu_{di/dt} + Z_{N\left(\mu_{di/dt},\sigma^2\right)}\sigma\{di/dt\}_{n,1-\alpha} \quad (21)$$

$$\chi^2\{dv/dt\}_{n-1,1-\alpha} = \mu_{dv/dt} + Z_{N\left(\mu_{dv/dt},\sigma^2\right)}\sigma\{dv/dt\}_{n,1-\alpha} \quad (22)$$

where $\mu_{di/dt}$ and $\mu_{dv/dt}$ are the means of the rates of change of current and voltage, respectively, as expressed in (23), $\sigma\{di/dt\}_{n,1-\alpha}$ and $\sigma\{dv/dt\}_{n,1-\alpha}$ are the standard deviations of the random variables di/dt and dv/dt, calculated by taking the positive square root of variances $\sigma^2\{di/dt\}_{n,1-\alpha}$ and $\sigma^2\{dv/dt\}_{n,1-\alpha}$ with the Chi-square-based confidence coefficient (1-α), respectively as expressed in (24) and (25), $Z_{N\left(\mu_{di/dt},\sigma^2\right)}$ and $Z_{N\left(\mu_{dv/dt},\sigma^2\right)}$ are the constant values obtained from the standard normal distribution table with the selected (1-α) confidence level, and $\chi^2_{n-1,1-\alpha}$ is a constant value, also acquired from the Chi-square distribution table.

$$\mu_{di/dt} = \sum_{j=i-99}^{i}\left(\frac{di_j}{dt}\right)\Big/100$$
$$\mu_{dv/dt} = \sum_{j=i-99}^{i}\left(\frac{dv_j}{dt}\right)\Big/100 \quad (23)$$

$$\sigma^2\{di/dt\}_{n,1-\alpha} = \sum_{i=1}^{n}\frac{\left(di_i/dt - \mu_{di/dt}\right)^2}{\chi^2_{n-1,1-\alpha}} \quad (24)$$

$$\sigma^2\{dv/dt\}_{n,1-\alpha} = \sum_{i=1}^{n}\frac{\left(dv_i/dt - \mu_{dv/dt}\right)^2}{\chi^2_{n-1,1-\alpha}} \quad (25)$$

B. Fault Detection for the LVDC MB based on the Cumulative Summation Algorithm

As seen in Figure 3, the second stage (Stage 2) of the proposed backup protection algorithm is to detect different faults in the LVDC MG due to the developed CS algorithm. The definite time integrals of current and voltage can be performed in discrete forms as expressed in (26) and (27).

$$S_i = \sum_{k=1}^{n} S_i(k) = \sum_{k=1}^{n} (i_k - \mu_i) \quad (26)$$

$$S_v = \sum_{k=1}^{n} S_v(k) = \sum_{k=1}^{n} (v_k - \mu_v) \quad (27)$$

where i_k and v_k represent the k^{th} measured value of the total n current and voltage samples, μ_i and μ_v are the sample means of the total n measurements, S_i and S_v are the sums of the deviations of the n current and voltage measurements from the mean value.

Generally, the upper and lower boundaries of S_i and S_v can be calculated from (28) and (29), where k_{emp} is an empirical factor depending on the level of confidence in fault detection. Note that n is selected to 100 for this study, which means that the first 100 consecutive samples are used to calculate the first values of thresholds $S_{i,LB}$, $S_{i,UB}$ $S_{v,LB}$, and $S_{v,UB}$. These thresholds will be properly updated for each following sample. Specifically, with n firstly consecutive samples from the 1st to the n^{th} samples, when either $S_i(n)$ or $S_v(n)$ are outside the range $\left[S_{i,LB}, S_{i,UB}\right], \forall k \in [1...n]$ or $\left[S_{v,LB}, S_{v,UB}\right], \forall k \in [1...n]$, respectively, it is implied that there is a short-circuit event in the DC system. Similarly, from the 2nd to the $(n+1)^{th}$ samples, if either $S_i(n+1)$or $S_v(n+1)$ are outside these ranges, there is also a fault in the DC MG.

$$\begin{cases} S_{i,UB} = \begin{cases} S_i(1) + ... + S_i(k-1) - (\mu_i + k_{emp}) \\ \quad \text{if } S_i(k) = i_k - \mu_i < 0, \forall k \in [1...n] \\ S_i(1) + ... + S_i(k-1) + S_i(k) - (\mu_i + k_{emp}) \\ \quad \text{if } S_i(k) = i_k - \mu_i > 0, \forall k \in [1...n] \end{cases} \\ S_{i,LB} = -S_{i,UB} \end{cases} \quad (28)$$

$$\begin{cases} S_{v,UB} = \begin{cases} S_v(1) + ... + S_v(k-1) - (\mu_v + k_{emp}) \\ \quad \text{if } S_v(k) = v_k - \mu_v < 0, \forall k \in [1...n] \\ S_v(1) + ... + S_v(k-1) + S_v(k) - (\mu_v + k_{emp}) \\ \quad \text{if } S_v(k) = v_k - \mu_v > 0, \forall k \in [1...n] \end{cases} \\ S_{v,LB} = -S_{v,UB} \end{cases} \quad (29)$$

C. Necessity of the Backup Protection with Failure of Circuit Breakers in the DC MG

A Circuit Breaker (CB) will be activated to isolate/clear the faulted position in the DC MG when it receives a tripping signal sent from the primary protection system. Failure of CBs means that they do not operate even if they already receive the tripping signal. The backup protection algorithm is proposed to determine whether the CBs fail to operate or not after a time delay t_d as expressed in (30), where the communication delay is denoted by t_{com}, the switching time of circuit breakers is denoted by t_{cb}, and the backup and primary protection times are defined by $t_{op,prim}$ and $t_{op,bkup}$, respectively. In case a failure of the main CB is detected, the tripping signal generated by the backup protection algorithm is sent back to the nearby circuit breakers to isolate the faulted section in the system.

$$t_{op,prim} + t_{op,bkup} + t_{cb} + t_{com} = t_d \quad (30)$$

D. The Necessity of Backup Protection of the Primary Algorithm

Primary protection relays should correctly detect the short-circuit events in the DC MG. Some common unit protection methods, e.g. current/voltage derivative-based protection methods with communication support, are proposed to mainly protect the DC MG due to their high sensitivity and selectivity, requiring the synchronization of measurement devices owing to the fast change of current and voltage. However, in case of communication failure, presence of noise in measurement systems, or damaged communication links, the backup protection algorithm must be activated to protect source and load branches in the DC MG. In other words, a fault event must be detected by the backup algorithm after a primary relay failure. It will send a tripping signal to the relevant CBs right after the sum of the primary protection time $t_{op,prim}$ along with t_{com} and t_{cb}.

After the time duration t_d, if the circuit breaker is successfully tripped, no more action is required. If the fault is not cleared, an alert signal is generated, and then the backup protection algorithm will continue to send the tripping signal to other nearby circuit breakers for fault isolation in the system. To ensure the high selectivity, scalability, and adaptability of the backup protection algorithm, this study has already proposed a novel backup protection scheme based on local measurements and Chi-square statistics for islanded LVDC MGs to timely detect and clear DC faults regardleess of variable fault resistances and damage of the communication.

E. Algorithm of the Proposed Backup Protection Scheme

As presented in Figure 3, at Stage 1, i.e. the abnormal detection of the LVDC MG even if a fault occurs, the backup protection algorithm will sample the k^{th} line current and voltage at the protected zones, i.e. source or load branches, with a sampling time interval of 0.001 s. By using n consecutive current/voltage samples from the i^{th} to $(i+n)^{th}$ samples in the moving data window, the protection algorithm will compute the following parameters:

- Chi-square statistical thresholds of current and voltage derivatives, with measurements from the i^{th} to the $(i+n)^{th}$ sample.
- The sum of deviations of the measured current and voltage signals, $S_i(k)$ and $S_v(k)$, $\forall k \in \left[i...(i+n)\right]$ from the CS algorithm.
- The upper and lower boundaries of S_i, as referred in (28).

- The upper and lower boundaries of S_v, as referred in (29).

After that, if the two following conditions:

$$\begin{cases} \dfrac{di_{i+n}}{dt}\left(=\dfrac{i_{i+n}-i_{i+n-1}}{\Delta t}\right) > \chi^2\{di/dt\}_{n-1,1-\alpha} \\ \dfrac{dv_{i+n}}{dt}\left(=\dfrac{v_{i+n}-v_{i+n-1}}{\Delta t}\right) > \chi^2\{dv/dt\}_{n-1,1-\alpha} \end{cases}$$

are not satisfied, the sampling process is continued and the statistical threshold calculations of the back-up protection algorithm are repeated. Otherwise, the protection algorithm will alert about an abnormal (fault or non-fault) operation of the DC MG, which has occurred in the system and will go to Stage 2, the fault detection in the LVDC MG. At this stage, the back-up protection algorithm continues to check the conditions $S_i(i+n) \notin \left[S_{i,LB}, S_{i,UB}\right]$ and $S_v(i+n) \notin \left[S_{v,LB}, S_{v,UB}\right]$. If they are not satisfied, it can be certainly concluded that a non-fault abnormal operation case of the DC MG has occurred and the algorithm could be repeated. Otherwise, a fault event in the DC MG can be effectively detected and the back-up protection algorithm will timely send tripping signals to relevant CBs to isolate the fault in the DC MG.

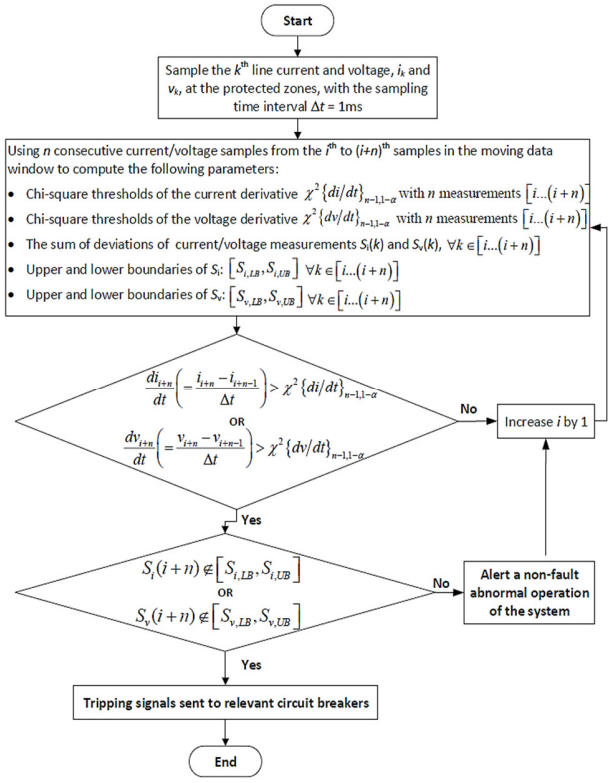

Fig. 3. Flowchart of the proposed backup fault protection scheme based on local measurements and Chi-square statistics for islanded LVDC MGs.

IV. MULTIPLE STAGED FAULT-TESTS ON A 1KW AND 48 V_{DC} OFF-GRID LVDC MG

The proposed backup protection algorithm was validated through multiple staged DC-fault tests in a real 1kW and 48 V_{DC} ungrounded DC-MG testbed. This DC-MG testbed includes: (i) two PV panels connected in series rated at 40.5 V_{DC}, 8A, and 1 kW in the standard condition, (ii) a 12~80 Vdc adjustable Boost Converter (BC) rated at 1000 W, 48 V_{DC}, and 20 A, (iii) a 1500 W and 48 V / 12 V-rated DC-DC bidirectional converter (BDC), (iv) a 12 V Li-ion battery pack, (v) resistive loads, and (vi) protective devices, such as DC fuses and solid-state relays, as portrayed in Figure 4.

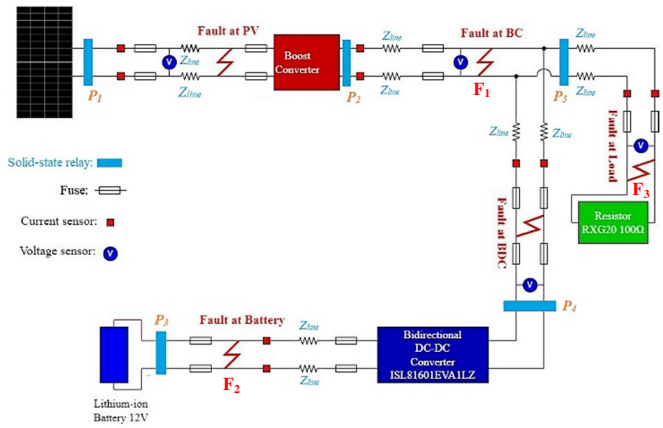

Fig. 4. Circuit diagram of an off-grid PV-battery-based 48 V_{DC} MG.

The line parameters of the off-grid testbed are 20 mΩ per km, line inductance is 100 μH per km, and the filter capacitor is 25 mF. Solid-state relays, P_1, P_2, P_3, P_4, and P_5 are used to mainly protect the PV modules, BC, battery pack, BDC, and resistive loads, respectively. In addition, fast-acting fuses are employed as backup protection devices for the mentioned relays. TM4C129ENCPDT microcontrollers were deployed to run the proposed backup protection algorithm, as seen in Figure 5. Two different fault locations, consisting of a faulted position on the DC-common bus (F1) and another at the load side (F3), are implemented to evaluate the performance of the proposed protection algorithm. Direct P2P faults (i.e. with a zero fault impedance) or low-impedance P2P faults are tested at these two faulty locations to check the possibility of the proposed protection scheme, i.e. the capability of timely detecting, accurately locating, and quickly clearing the DC faults within the expected time frame. Table I summarizes the main design parameters of the small-sized offgrid 48 V_{dc} DC-MG testbed.

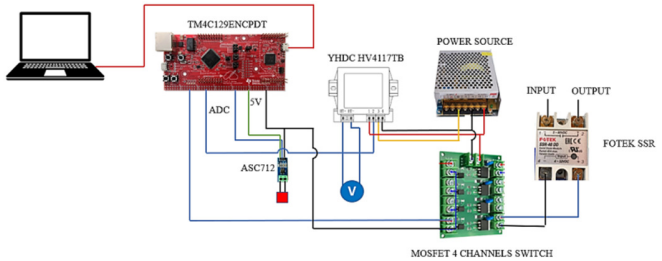

Fig. 5. Typical circuit diagram of a current and voltage measurement system in the studied DC MG.

TABLE I. MAIN PARAMETERS OF THE TESTBED

Main components	Descriptions
1. Two series-connected PV modules	In the standard test condition, each PV module has the following: • Maximum power of 500 W • Operating voltage of 40.5 V_{DC} • Operating current of 8 A • Open-circuit voltage of 49.5 V • Short-circuit current of 10.5 A • Efficiency of about 20%
2. One adjustable BC for PV modules	• Input voltage range: 12~80 V_{DC} • Output voltage: 48 V_{DC} • Rated power: 1000 W • Rated input current: 20 A • Switching frequency: 150 kHz • Conversion efficiency: 92% ~ 97% • Internal overcurrent protection
3. One DC-DC BDC (Renesas ISL81601EVAL1Z)	• Voltage at the DC-bus side: 48 V_{DC} • Voltage at the battery side: 12 V_{DC} • Rated power: 1500 W • Switching frequency : 100 kHz to 600 kHz • Internal overcurrent protection
4. One Li-ion battery pack	• Operating voltage of the battery: 12 V_{DC} • Rated capacity: 20 Ah
5. Resistive loads (RXG20)	• Resistance levels from 1W to 100W • High power ratings (up to 15 kW) and operating voltages (up to 1.2 kV) • Terminals are connected by bolts or solder
6. Protective devices	There are about 16 DC fuses, rated by: • Number of poles: 2 • Rated voltage: 500 V • Rated current: 10 A or 20 A There are five solid-state relays, rated by: • Voltage range: 5 ~ 60 V_{DC} • Maximum current: 100 A • Activated voltage range: 3 ~ 32 V_{DC}
7. Measurement devices	There are 10 current sensors, rated by: • Measured current range: 0 ~ 100 A • Bandwidth: 80 kHz • Output sensitivity: 66 ~185 mV/A • Low-noise analog signal path There are 5 voltage sensors (YHDCHV4117TB), rated by: • Rated votlage input: 0 ~ 500 V_{DC} • Output votlage range: 0 ~ 5 V_{DC} • Load impedance: ≥ 10 kΩ • Supply voltage: ±12V/±15V • Response time: 40 ~ 200 μs
8. Microcontroller	A TM4C129ENCPDT Texas Instruments microcontroller is used to implement the proposed backup protection algorithm. This unit has a 120 MHz Arm Cortex-M4F CPU, 1 MB of flash, and 256 kB of SRAM. It also has two 12-bit ADC modules, PWM and QEI modules, several serial communication channels for UART, SPI, I2C, and CAN.
9. Line parameters	• Line resistance: 20 mΩ per km • Line inductance:100 μH per km • Filter capacitors: 25 mF

V. EXPERIMENTAL RESULTS, ANALYSIS, AND DISCUSSION

In this section, the numerical results from multiple fault tests on the off-grid testbed will be presented and discussed. For each chart of the results, its title denotes the following information in the following unified order: "*battery operation state, fault type, faulted location, subject of the chart*". The battery operation state can be either charging or discharging, whereas the fault type can either be a direct P2P fault or a low-impedance P2P fault. The faulted location can be either the position of the common bus (F1) or the position of the load branch (F3). The subjects of the chart are the measured/calculated parameters, as mentioned in the backup protection algorithm in Figure 3. For example, a chart with the name "*Charging, direct P2P fault, F1,* di/dt *&* $\chi^2\{di/dt\}_{n-1,1-\alpha}$" means that while the battery system of the off-grid 48 V_{DC} MG testbed is being charged, a direct P2P fault occurs at the position of DC-common bus, and the waveforms of two parameters, di/dt and $\chi^2\{di/dt\}_{n-1,1-\alpha}$, measured/ calculated by the proposed backup protection algorithm are shown.

A. P2P Fault Detection Results at F1

Figure 6 illustrates the fault detection results when a direct P2P fault occurs at the DC-common bus (F1). The backup protection algorithm will send a tripping signal to the relay P_2 to isolate the PV BC from the faulted location. The time parameters t_{ini} and t_{fin} are the fault inception and clearing time, respectively, determined by the backup protection algorithm. During the fault event, both di/dt and dv/dt exceed their Chi-square thresholds of around 2000 A/s and 35000 V/s, respectively. In addition, two conditions, $S_i(i+n) \notin \left[S_{i,LB}, S_{i,UB}\right]$ and $S_v(i+n) \notin \left[S_{v,LB}, S_{v,UB}\right]$ are also satisfied. The signals $S_i(k)$ and $S_v(k)$ are outside the ranges $\left[S_{i,LB}, S_{i,UB}\right]$ and $\left[S_{v,LB}, S_{v,UB}\right]$, respectively, as referred to Table II. As a result, the backup algorithm can detect and clear the direct P2P fault within 3 ms, and thus protect the PV source branch in the DC system.

Figures 7 and 8 display the fault detection results when a direct P2P fault with a zero fault impedance occurs at F1. The backup protection algorithm will send a tripping signal to the relay P_4 to isolate the BDC from the faulted location irrespective of the charging or discharging state of the battery system. Consequently, as referred to Table II, the conditions:

$$di/dt > \chi^2\{di/dt\}_{n-1,1-\alpha},$$

$$dv/dt > \chi^2\{dv/dt\}_{n-1,1-\alpha}, \text{ and}$$

$$\begin{cases} S_i(i+n) \notin \left[S_{i,LB}, S_{i,UB}\right] \\ S_v(i+n) \notin \left[S_{v,LB}, S_{v,UB}\right] \end{cases},$$

are all satisfied to effectively identify the direct P2P fault at the position F1 in the testbed. The total time for fault detection and isolation is mostly about 3 ms, which is within the expected time frame. In conclusion, the continuously–updated Chi-square thresholds are properly used to detect the abnormal operation of the LVDC MG, while the cumulative summation method of line current and voltage is appropriately utilized to determine fault-tripping thresholds in the backup protection for detecting many severe faults within a few milliseconds.

Table II summarises the experimental results achieved for the proposed back-up DC-MG protection with respect to the direct P2P fault event at the DC common bus (F1). Note that the faulted bus position F1 is the most serious short-circuit occurrence of the LVDC MG wherein all source and energy-storage branches are mostly susceptible with this direct P2P fault type. Regardless the large transients and measurement noises of the fault current and voltage during the standalone operation of the 48 V_{DC} MG testbed, the direct P2P fault at the common DC-bus can be detected and cleared within a few milliseconds.

TABLE II. SUMMARY AND DISCUSSION OF THE EXPERIMENTAL RESULTS OF THE PROPOSED BACK-UP PROTECTION WITH REGARD TO A DIRECT P2P FAULT AT THE DC COMMON BUS (F1) OF THE TESTBED

Protection cases of the MG	**A direct pole-to-pole fault at the common DC-bus F1 of the off-grid 48V_{DC} microgrid testbed**					
	Abnormal detection based on Chi-square statistics		**Fault detection based on the CS algorithm**		**Fault clearing time**	**Discussion**
	Chi-square-based thresholds, $\chi^2\{di/dt\}_{n-1,1-\alpha}$ $\chi^2\{dv/dt\}_{n-1,1-\alpha}$	Actual values of di/dt and dv/dt	Calculated tripping thresholds, $[S_{i,LB}, S_{i,UB}]$ $[S_{v,LB}, S_{v,UB}]$	Actual values of $S_i(k)$ and $S_v(k)$		When the direct P2P fault occurs at the common bus (F1), the output capacitor of the PV BC discharges very fast to the faulted position, therefore, the change of the current and voltage with respect to time is very high, such that the abnormal operation of the DC MG can be detected quickly and effectively within 1 ms. Then, the values of $S_i(k)$ and $S_v(k)$ exceed their CS-based tripping thresholds. Consequently, the SSR at the position P2 as indicated in Figure 4 is very quickly activated to isolate the faulted position F1 and to protect the PV-source branch within the expected time of 3 ms. By comparing with the methods presented in [23, 28, 29], the proposed back-up protection scheme is superior in protecting the PV-source branch in the DC MG in the case of any failure of circuit breakers or primary protection functions in the DC system.
1. Protection results of the PV-source branch	2000 A/s and 35000 V/s right before the fault inception time	2900 A/s and 44000 V/s after 1 ms from the fault time	[-1 A, +1 A] and [-5 V, +5 V] right before the fault inception time	+5 A and -44 V after 1 ms from the fault time	3 ms	
2. Protection results of the battery source branch under charging operation	380 A/s and 34000 V/s right before the fault inception time	1900 A/s 41000 V/s after 1 ms from the fault time	[-1 A, +1 A] and [-11 V, +11 V] right before the fault inception time	+2 A and -42 V after 1 ms from the fault time	3 ms	The charging current is negative while the discharging current is positive as seen in Figures 7 and 8, respectively. Regardless of the charging and discharging modes of the BESS branch, the proposed backup protection can detect and clear very quickly the direct P2P fault occurrence at the common bus (F1). The output capacitor of the battery BDC contributes a high fault current to F1, so the di/dt and dv/dt values are very high to identify the abnormal operation, and the $\begin{cases} S_i(i+n) \notin [S_{i,LB}, S_{i,UB}] \\ S_v(i+n) \notin [S_{v,LB}, S_{v,UB}] \end{cases}$ constraints are correct. As a result, the SSR at the position P4 is timely activated to protect the BESS branch from the direct P2P fault F1 within 2 ~ 5 ms right after the fault inception, as similar to the fault clearing time of other protection methods in [8, 22, 23, 28, 29, 35].
3. Protection results of the battery source branch under discharging operation	600 A/s and 34000V/s right before the fault inception time	2500 A/s and 44000V/s after 1ms from the fault time	[-1.7 A, +1.7 A] and [-3 V, +3 V] right before the fault inception time	+2 A and -44 V after 1 ms from the fault time	3 ms	

B. (P2P) Fault Detection Results at F3

1) Direct P2P Fault Detection Results

Figure 9 presents the fault detection results of the backup protection algorithm to protect the load branch of the DC MG with respect to a direct P2P fault at F3. As seen in Figure 9(a)-(b), the change rates of the current and voltage experienced transient responses of extremely high values when the direct P2P fault occurred at the load branch (F3). Typically, di/dt reached up to 2300 A/s and dv/dt surpassed 40000 V/s after 2 ms the fault inception time, exceeding both their Chi-square statistical thresholds, i.e. the two conditions of the algorithm are both satisfied. Consequently, the proposed backup protection can properly detect the abnormal operation of the load branch of the DC MG within three locally consecutive sample points of the current and voltage right after the fault occurrence.

Regarding the cumulative-summation-algorithm-based tripping thresholds of the line current and voltage, it can be manifested in Figure 9(c)-(d) that, right after the fault event, the current-related signal $S_i(k)$ quickly increases to almost 3 A and outside the range of $[S_{i,LB}, S_{i,UB}]$. Similarly, the voltage-related signal $S_v(k)$ also significantly drops outside the range of $[S_{v,LB}, S_{v,UB}]$ within two consecutive samples immediately after the fault occurrence at F3. As a result, based on the upper and lower boundaries of the cumulative summation of current and voltage, the backup protection algorithm can successfully detect the direct P2P fault at F3 in the DC MG testbed within the expected time of about 3 ms.

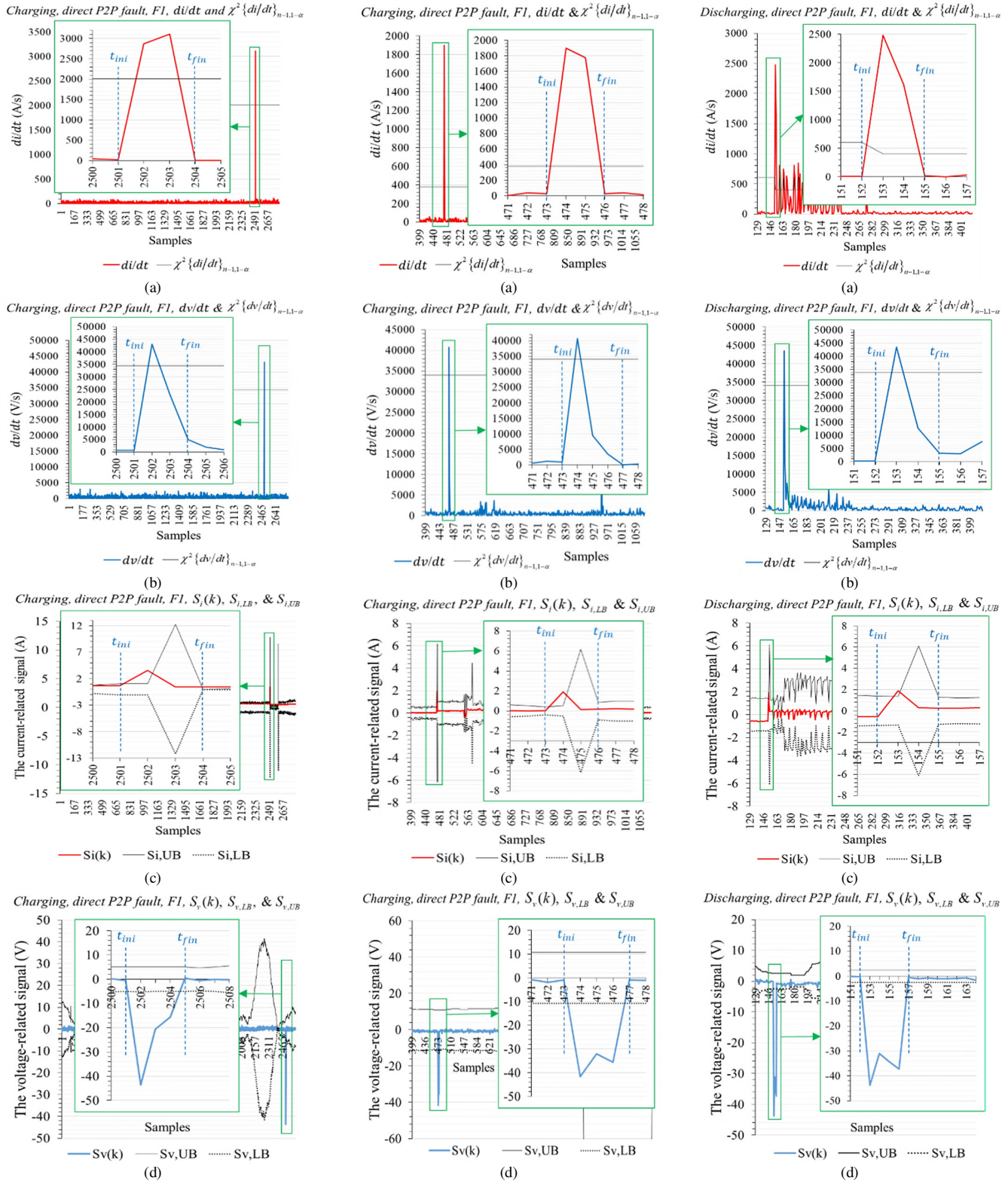

Fig. 6. Transient response of parameters/thresholds in the backup protection algorithm to protect the PV BC regarding a direct P2P fault at the common bus (F1) of the DC-MG testbed.

Fig. 7. Transient response of parameters/ thresholds in the backup protection algorithm to protect the charged battery system regarding a direct P2P fault at F1.

Fig. 8. Transient response of parameters/ thresholds in the backup protection algorithm to protect the discharged battery system regarding a direct P2P fault at F1.

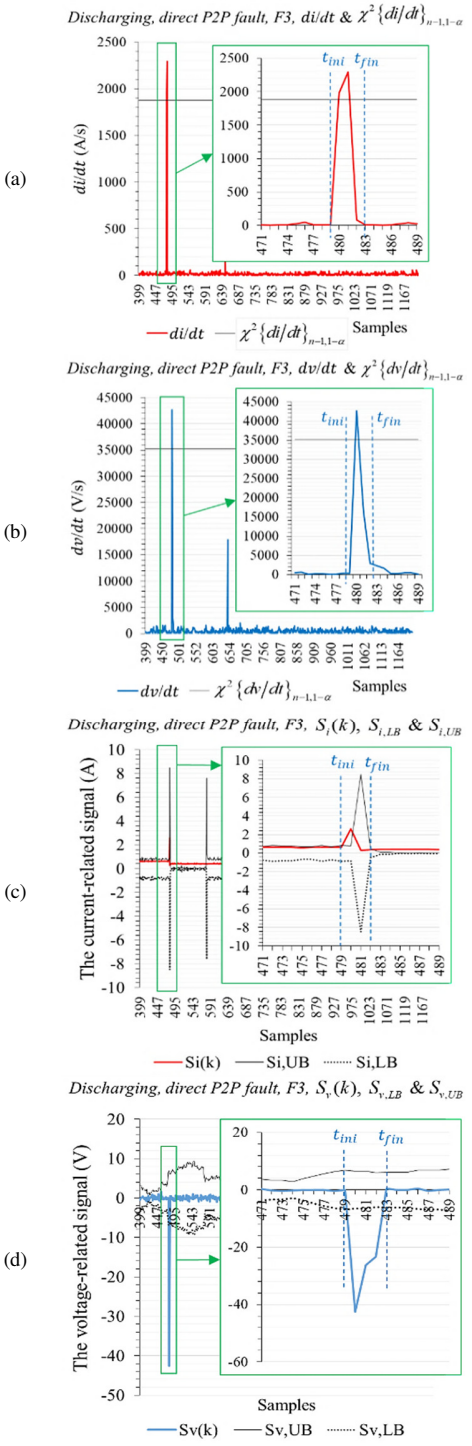

Fig. 9. Transient response of parameters/ thresholds in the backup protection algorithm regarding a direct P2P fault at F3 of the testbed.

2) Low-Impedance P2P Fault Detection Results

Figure 10 depicts the short-circuit detection results of the backup protection algorithm with respect to a Low-Impedance (LI) P2P fault at F3. In general, either the condition $di/dt > \chi^2\{di/dt\}_{n-1,1-\alpha}$ or $dv/dt > \chi^2\{dv/dt\}_{n-1,1-\alpha}$, and either the condition $S_i(i+n) \notin \left[S_{i,LB}, S_{i,UB}\right]$ or $S_v(i+n) \notin \left[S_{v,LB}, S_{v,UB}\right]$ are satisfied to effectively identify the low-impedance P2P fault at the position of F3 in the DC MG testbed.

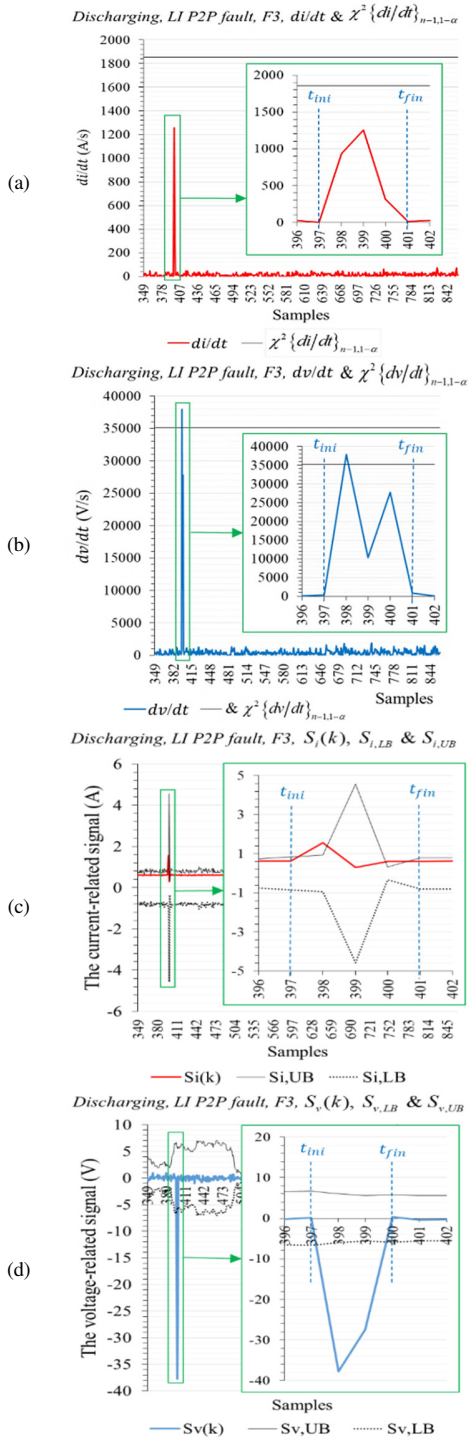

Fig. 10. Transient response of parameters/ thresholds in the backup protection algorithm regarding an LI P2P fault at F3 of the testbed.

TABLE III. SUMMARY AND DISCUSSION ON THE EXPERIMENTAL RESULTS WITH RESPECT TO DIRECT AND LI P2P FAULTS IN THE LOAD BRANCH (F3) OF THE TESTBED

Protection cases of the MG	**Abnormal detection based on Chi-square statistics**		**Fault detection based on the CS algorithm**		**Fault clearing time**	**Discussion**
	Chi-square-based thresholds, $\chi^2\{di/dt\}_{n-1,1-\alpha}$ $\chi^2\{dv/dt\}_{n-1,1-\alpha}$	Actual values of di/dt and dv/dt	Calculated tripping thresholds, $[S_{i,LB}, S_{i,UB}]$ $[S_{v,LB}, S_{v,UB}]$	Actual values of $S_i(k)$ and $S_v(k)$		
Protection results of the load branch of the LVDC MG	**Case 1: A direct P2P fault at the load branch (F3)**					Relays at positions P2, P4, and P5 can identify the direct/low-impedance P2P faults at F3 because the change rate of current or voltage exceeds its Chi-square statistical threshold, and the conditions of the algorithm are satisfied. Tripping operations of P2, P4, and P5 are determined by a coordination time interval of 5 ms. In case all P2, P4, and P5 simultaneously find out the P2P fault event at F3, the relay P5 will be firstly activated to protect the load branch. If the P2P fault at F3 still remains until 5 ms after the fault inception time, the relays P2 and P4 will be then activated to clear this fault. This time interval-based protection coordination is suitable with the off-grid and small-scale LVDC MG instead of using communication links to coordinate the devices P2, P4, P5 as presented in [8, 20, 25-27, 41]. The SSR, P5, is timely activated to protect the load branch from the direct/LI P2P faults within 2 ~ 5ms right after the fault inception, as similar to the fault clearing time of the MG protection methods in [28, 29, 35].
	1800 A/s and 35000 V/s right before the fault inception time	2300 A/s and 43000 V/s after 1 ms from the fault time	[-0.9 A, +0.9 A] and [-6 V, +6 V] right before the fault inception time	+3 A and -44 V after 1 ms from the fault time	3 ms	
	Case 2: An LI P2P fault at the load branch (F3)					
	1950 A/s & 35000 V/s right before the fault inception time	900 A/s & 38000 V/s after 1ms from the fault time	[-0.9 A, +0.9 A] and [-6 V, +6 V] right before the fault inception time	+1.2 A and -38 V after 1 ms from the fault time	3 ms	

The total time of fault detection and isolation is about 4 ms, which is within the expected time frame. It can be noted that in some cases of the LI-P2P faults, either $di/dt > \chi^2\{di/dt\}_{n-1,1-\alpha}$ or $dv/dt > \chi^2\{dv/dt\}_{n-1,1-\alpha}$ is satisfied to identify the abnormal operation of the system instead of both because the non-zero fault impedance could significantly limit the magnitude of short-circuit currents in the MG.

Table III summarizes the achieved experimental results of the proposed back-up DC-MG protection with respect to direct and LI P2P fault events at the load branch (F3). Note that current and voltage signals are locally sampled for their Chi-square statistical calculation to detect any abnormal operation of the load branch, then tripping thresholds adaptably calculated by the CS algorithm are used to accurately detect the P2P faults at F3. Regardless of the large transients and measurement noises of the fault current and voltage during the operation of the testbed, the direct and LI P2P faults at F3 can be detected and cleared within the expected time range of 3 ~ 5 ms.

VI. CONCLUSIONS AND FUTURE WORK

To avoid any communication failures of differential-current-based, overcurrent-based, current/voltage-derivative-based primary protection methods or damage of circuit breakers, this paper comprehensively presents a novel backup protection algorithm for offgrid LVDC MGs. This backup protection implements local measurements of the line current and voltage without the communication support, calculates Chi-square-distribution-relied statistical thresholds for the abnormal operation detection of the MG, and determines fault-tripping thresholds based on the cumulative summation method of current and voltage signals to effectively detect different fault types, i.e. direct and LI P2P faults, in the off-grid LVDC MG. The experimental results revealed that the proposed backup protection uses Chi-square thresholds to initially detect the abnormal operation of the LVDC MG within 2 ms from the inception time, and then employs the cumulative summation algorithm to determine the adaptable fault-tripping thresholds for accurately detecting and quickly removing faults in the system in the expected time frame of 2 ~ 5ms. The back-up protection algorithm is less sensitive to the measurement noise, capable of accurately detecting severe P2P faults and protects the source and load branches within the expected time frame of a few milliseconds. Staged fault-testing results from a real-time ungrounded 1 kW and 48 V_{DC} MG testbed demonstrated the effectiveness of the developed scheme. In the future, more staged tests of load shifting, and dynamic change cases of sources and loads in a real-time LVDC MG testbed could be conducted to further validate the effectiveness of the proposed backup protection in detecting and classifying between high-impedance faults and dynamic operations of the LVDC MG. Besides that, simulation cases with more random fault and dynamic operation scenarios of the LVDC MG from the PSCAD/EMTDC or RSCAD software could be implemented to validate the adaptability, scalability, and selectivity of the developed back-up protection scheme.

ACKNOWLEDGMENT

The authors thank Le Hoang Khang, Huynh Thanh Tung, and Nguyen Minh Hieu at the Vietnamese-German University (VGU), Vietnam, for supporting the experimental data processing from the 48 V_{DC} off-grid PV-battery microgrid testbed.

REFERENCES

[1] S. Muchande and S. Thale, "Hierarchical Control of a Low Voltage DC Microgrid with Coordinated Power Management Strategies," *Engineering, Technology & Applied Science Research*, vol. 12, no. 1, pp. 8045–8052, Feb. 2022, https://doi.org/10.48084/etasr.4625.

[2] M. E. Baran and N. R. Mahajan, "Overcurrent Protection on Voltage-Source-Converter-Based Multiterminal DC Distribution Systems," *IEEE Transactions on Power Delivery*, vol. 22, no. 1, pp. 406–412, Jan. 2007, https://doi.org/10.1109/TPWRD.2006.877086.

[3] D. M. Bui, S.-L. Chen, C.-H. Wu, K.-Y. Lien, C.-H. Huang, and K.-K. Jen, "Review on protection coordination strategies and development of an effective protection coordination system for DC microgrid," in *IEEE PES Asia-Pacific Power and Energy Engineering Conference*, Hong Kong, China, Dec. 2014, pp. 1–10, https://doi.org/10.1109/APPEEC.2014.7066159.

[4] D. M. Bui, P. D. Le, and T. D. Nguyen, "Staged Fault Tests to Validate a Fast Protection System of Low-Voltage DC Microgrids," in *International Conference on Electrical, Computer, Communications and Mechatronics Engineering*, Mauritius, Mauritius, Oct. 2021, pp. 1–6, https://doi.org/10.1109/ICECCME52200.2021.9591112.

[5] R. M. Cuzner and G. Venkataramanan, "The Status of DC Micro-Grid Protection," in *IEEE Industry Applications Society Annual Meeting*, Edmonton, AB, Canada, Oct. 2008, pp. 1–8, https://doi.org/10.1109/08IAS.2008.382.

[6] S. D. A. Fletcher, P. J. Norman, S. J. Galloway, P. Crolla, and G. M. Burt, "Optimizing the Roles of Unit and Non-unit Protection Methods Within DC Microgrids," *IEEE Transactions on Smart Grid*, vol. 3, no. 4, pp. 2079–2087, Sep. 2012, https://doi.org/10.1109/TSG.2012.2198499.

[7] A. Meghwani, S. C. Srivastava, and S. Chakrabarti, "A Non-unit Protection Scheme for DC Microgrid Based on Local Measurements," *IEEE Transactions on Power Delivery*, vol. 32, no. 1, pp. 172–181, Oct. 2017, https://doi.org/10.1109/TPWRD.2016.2555844.

[8] A. Shabani and K. Mazlumi, "Evaluation of a Communication-Assisted Overcurrent Protection Scheme for Photovoltaic-Based DC Microgrid," *IEEE Transactions on Smart Grid*, vol. 11, no. 1, pp. 429–439, Jan. 2020, https://doi.org/10.1109/TSG.2019.2923769.

[9] A. A. Bakar *et al.*, "Decentralized Virtual Impedance-based Circulating Current Suppression Control for Islanded Microgrids," *Engineering, Technology & Applied Science Research*, vol. 11, no. 1, pp. 6734–6739, Feb. 2021, https://doi.org/10.48084/etasr.3895.

[10] G. K. Rao and P. Jena, "Unit Protection of Tapped Line DC Microgrid," *IEEE Journal of Emerging and Selected Topics in Power Electronics*, vol. 10, no. 4, pp. 4680–4689, Dec. 2022, https://doi.org/10.1109/JESTPE.2022.3143525.

[11] M. Farhadi and O. A. Mohammed, "Event-Based Protection Scheme for a Multiterminal Hybrid DC Power System," *IEEE Transactions on Smart Grid*, vol. 6, no. 4, pp. 1658–1669, Jul. 2015, https://doi.org/10.1109/TSG.2015.2396995.

[12] X. Feng, L. Qi, and J. Pan, "A Novel Fault Location Method and Algorithm for DC Distribution Protection," *IEEE Transactions on Industry Applications*, vol. 53, no. 3, pp. 1834–1840, Feb. 2017, https://doi.org/10.1109/TIA.2017.2666083.

[13] R. Moxley and K. Fodero, "High-speed distribution protection made easy: communications-assisted protection schemes for distribution applications," in *58th Annual Conference for Protective Relay Engineers*, College Station, TX, USA, Apr. 2005, pp. 18–26, https://doi.org/10.1109/CPRE.2005.1430418.

[14] S. D. A. Fletcher, P. J. Norman, K. Fong, S. J. Galloway, and G. M. Burt, "High-Speed Differential Protection for Smart DC Distribution Systems," *IEEE Transactions on Smart Grid*, vol. 5, no. 5, pp. 2610–2617, Sep. 2014, https://doi.org/10.1109/TSG.2014.2306064.

[15] S. Dhar, R. K. Patnaik, and P. K. Dash, "Fault Detection and Location of Photovoltaic Based DC Microgrid Using Differential Protection Strategy," *IEEE Transactions on Smart Grid*, vol. 9, no. 5, pp. 4303–4312, Sep. 2018, https://doi.org/10.1109/TSG.2017.2654267.

[16] A. Meghwani, S. C. Srivastava, and S. Chakrabarti, "A new protection scheme for DC microgrid using line current derivative," in *IEEE Power & Energy Society General Meeting*, Denver, CO, USA, Jul. 2015, pp. 1–5, https://doi.org/10.1109/PESGM.2015.7286041.

[17] A. A. S. Emhemed, K. Fong, S. Fletcher, and G. M. Burt, "Validation of Fast and Selective Protection Scheme for an LVDC Distribution Network," *IEEE Transactions on Power Delivery*, vol. 32, no. 3, pp. 1432–1440, Jun. 2017, https://doi.org/10.1109/TPWRD.2016.2593941.

[18] R R. Eslami, S. H. H. Sadeghi, and H. A. Abyaneh, "A Probabilistic Approach for the Evaluation of Fault Detection Schemes in Microgrids," *Engineering, Technology & Applied Science Research*, vol. 7, no. 5, pp. 1967–1973, Oct. 2017, https://doi.org/10.48084/etasr.1472.

[19] L. B. Raju and K. S. Rao, "Evaluation of Passive Islanding Detection Methods for Line to Ground Unsymmetrical Fault in Three Phase Microgrid Systems: Microgrid Islanding Detection Method," *Engineering, Technology & Applied Science Research*, vol. 11, no. 5, pp. 7591–7597, Oct. 2021, https://doi.org/10.48084/etasr.4310.

[20] R. Mohanty, S. Sahoo, A. K. Pradhan, and F. Blaabjerg, "A Cosine Similarity-Based Centralized Protection Scheme for dc Microgrids," *IEEE Journal of Emerging and Selected Topics in Power Electronics*, vol. 9, no. 5, pp. 5646–5656, Jul. 2021, https://doi.org/10.1109/JESTPE.2021.3060587.

[21] N. Bayati, H. R. Baghaee, A. Hajizadeh, M. Soltani, Z. Lin, and M. Savaghebi, "Local Fault Location in Meshed DC Microgrids Based On Parameter Estimation Technique," *IEEE Systems Journal*, vol. 16, no. 1, pp. 1606–1615, Mar. 2022, https://doi.org/10.1109/JSYST.2021.3107905.

[22] S. Augustine, M. J. Reno, S. M. Brahma, and O. Lavrova, "Fault Current Control and Protection in a Standalone DC Microgrid Using Adaptive Droop and Current Derivative," *IEEE Journal of Emerging and Selected Topics in Power Electronics*, vol. 9, no. 3, pp. 2529–2539, Jun. 2021, https://doi.org/10.1109/JESTPE.2020.2984609.

[23] G. K. Rao and P. Jena, "A Novel Fault Identification and Localization Scheme for Bipolar DC Microgrid," *IEEE Transactions on Industrial Informatics*, vol. 19, no. 12, pp. 11752–11764, Dec. 2023, https://doi.org/10.1109/TII.2023.3252409.

[24] S. Sanati, A. Mosayebi, and I. Kamwa, "Advanced Rapid Directional Over-Current Protection for DC Microgrids Using K-Means Clustering," *IEEE Transactions on Power Delivery*, vol. 39, no. 2, pp. 1088–1099, Apr. 2024, https://doi.org/10.1109/TPWRD.2024.3353109.

[25] S. Ahmadi, I. Sadeghkhani, G. Shahgholian, B. Fani, and J. M. Guerrero, "Protection of LVDC Microgrids in Grid-Connected and Islanded Modes Using Bifurcation Theory," *IEEE Journal of Emerging and Selected Topics in Power Electronics*, vol. 9, no. 3, pp. 2597–2604, Jun. 2021, https://doi.org/10.1109/JESTPE.2019.2961903.

[26] A. Saxena, N. K. Sharma, and S. R. Samantaray, "An Enhanced Differential Protection Scheme for LVDC Microgrid," *IEEE Journal of Emerging and Selected Topics in Power Electronics*, vol. 10, no. 2, pp. 2114–2125, Apr. 2022, https://doi.org/10.1109/JESTPE.2022.3144300.

[27] M. W. Altaf *et al.*, "Control and Protection Scheme for DC-Link of Solar PV Based Microgrid," *IEEE Transactions on Industry Applications*, vol. 60, no. 2, pp. 2706–2715, Mar. 2024, https://doi.org/10.1109/TIA.2023.3341848.

[28] L. Kong and H. Nian, "Fault Detection and Location Method for Mesh-Type DC Microgrid Using Pearson Correlation Coefficient," *IEEE Transactions on Power Delivery*, vol. 36, no. 3, pp. 1428–1439, Jun. 2021, https://doi.org/10.1109/TPWRD.2020.3008924.

[29] G. K. Rao and P. Jena, "Fault Detection in DC Microgrid Based on the Resistance Estimation," *IEEE Systems Journal*, vol. 16, no. 1, pp. 1009–1020, Mar. 2022, https://doi.org/10.1109/JSYST.2020.3046054.

[30] M. A. Jarrahi, H. Samet, and T. Ghanbari, "Fault Detection in DC Microgrid: A Transient Monitoring Function-Based Method," *IEEE Transactions on Industrial Electronics*, vol. 70, no. 6, pp. 6284–6294, Jun. 2023, https://doi.org/10.1109/TIE.2022.3194580.

[31] M. R. K. Rachi, M. A. Khan, and I. Husain, "Local Measurement-Based Protection Coordination System for a Standalone DC Microgrid," *IEEE Transactions on Industry Applications*, vol. 57, no. 5, pp. 5332–5344, Sep. 2021, https://doi.org/10.1109/TIA.2021.3091945.

[32] N. Bayati, H. R. Baghaee, A. Hajizadeh, and M. Soltani, "Localized Protection of Radial DC Microgrids With High Penetration of Constant

Power Loads," *IEEE Systems Journal*, vol. 15, no. 3, pp. 4145–4156, Sep. 2021, https://doi.org/10.1109/JSYST.2020.2998059.

[33] M. W. Altaf, M. T. Arif, S. N. Islam, and Md. E. Haque, "Microgrid Protection Challenges and Mitigation Approaches-A Comprehensive Review," *IEEE Access*, vol. 10, pp. 38895–38922, Jan. 2022, https://doi.org/10.1109/ACCESS.2022.3165011.

[34] Z. Ali *et al.*, "Fault Management in DC Microgrids: A Review of Challenges, Countermeasures, and Future Research Trends," *IEEE Access*, vol. 9, pp. 128032–128054, Jan. 2021, https://doi.org/10.1109/ACCESS.2021.3112383.

[35] C. Srivastava and M. Tripathy, "Novel Adaptive Fault Detection Strategy in DC Microgrid Utilizing Statistical-Based Method," *IEEE Transactions on Industrial Informatics*, vol. 19, no. 5, pp. 6917–6929, May 2023, https://doi.org/10.1109/TII.2022.3199942.

[36] S. Ravyts, G. V. den Broeck, L. Hallemans, M. D. Vecchia, and J. Driesen, "Fuse-Based Short-Circuit Protection of Converter Controlled Low-Voltage DC Grids," *IEEE Transactions on Power Electronics*, vol. 35, no. 11, pp. 11694–11706, Nov. 2020, https://doi.org/10.1109/TPEL.2020.2988087.

[37] S. A. Wakode, M. S. Ballal, A. A. Sheikh, and R. R. Deshmukh, "Oscillation Frequency Component-Based Protection Scheme for DC Microgrid," *IEEE Transactions on Industry Applications*, vol. 57, no. 6, pp. 5747–5757, Nov. 2021, https://doi.org/10.1109/TIA.2021.3115089.

[38] S. K. Prince, S. Affijulla, and G. Panda, "Protection of DC Microgrids Based on Complex Power During Faults in On/Off-Grid Scenarios," *IEEE Transactions on Industry Applications*, vol. 59, no. 1, pp. 244–254, Jan. 2023, https://doi.org/10.1109/TIA.2022.3206171.

[39] S. D. A. Fletcher, P. J. Norman, S. J. Galloway, and G. M. Burt, "Determination of protection system requirements for DC unmanned aerial vehicle electrical power networks for enhanced capability and survivability," *IET Electrical Systems in Transportation*, vol. 1, no. 4, pp. 137–147, Dec. 2011, https://doi.org/10.1049/iet-est.2010.0070.

[40] A. Meghwani, R. Gokaraju, S. C. Srivastava, and S. Chakrabarti, "Local Measurements-Based Backup Protection for DC Microgrids Using Sequential Analyzing Technique," *IEEE Systems Journal*, vol. 14, no. 1, pp. 1159–1170, Mar. 2020, https://doi.org/10.1109/JSYST.2019.2919144.

[41] H. Eid, H. M. Sharaf, and M. Elshahed, "Optimal Protection Coordination of Directional Overcurrent Relays in Microgrids considering Grid- Connected and Islanded Modes based on User defined Characteristics and Fault Current Limiters," *International Journal of Renewable Energy Research*, vol. 12, no. 4, pp. 1932–1941, Dec. 2022, https://doi.org/10.20508/ijrer.v12i4.13449.g8616.

AUTHORS PROFILE

Duong Minh Bui received the B.S. degree in Electrical Engineering at Can Tho University, Vietnam in 2008; the M.Sc. degree in Electrical Power Engineering at the University of Greenwich, UK in 2012; and the Ph.D. degree in Electrical Power Engineering at Chung Yuan Christian University, Taiwan in 2017. He was a postdoctoral researcher at Taiwan Power Company in the period 2016 - 2017, Taiwan. He is currently a lecturer in electrical power engineering at Vietnamese-German University (VGU), Vietnam. His research interests are the protection system design of AC and DC microgrids, reliability analysis of the microgrid, load forecasting, and technical-economic assessment of renewable energy sources.

Phuc Duy Le was born in Ho Chi Minh City (HCMC), Viet Nam, in 1991. He received the B.S. degree in Electrical Engineering at HCMC University of Industry (IUH) in 2013 and the M.S. and Ph.D. degrees in Electrical Engineering at HCMC University of Technology (HUTECH), Vietnam, in 2016 and 2021, respectively. Currently, he is vice director of Phu Tho Power Company at Ho Chi Minh City, Ho Chi Minh Power Corporation (EVNHCMC), Viet Nam, and is an adjunct lecturer at Industrial University of Ho Chi Minh City, Ho Chi Minh City, Vietnam. His research interests are protection, control automation, and artificial intelligence in smart distribution networks.

Hieu Minh Nguyen was born in Ho Chi Minh City (HCMC), Viet Nam. received the B.S. degree in Electrical Engineering and Information Technology at Vietnamese-German University (VGU), Vietnam and Frankfurt University of Applied Sciences in 2019. Now, he is working for the M.S. degree in Global Production Engineering and Management at Vietnamese-German University, Vietnam. He is a lab engineer in Automation and Control Engineering at VGU. His research interests are the protection system design of AC and DC microgrids, reliability analysis and technical-economic assessment of renewable energy sources, and energy economics.